



HAL
open science

The effects of outgassing on the transition between effusive and explosive silicic eruptions

Wim Degruyter, Olivier Bachmann, Alain Burgisser, M. Manga

► **To cite this version:**

Wim Degruyter, Olivier Bachmann, Alain Burgisser, M. Manga. The effects of outgassing on the transition between effusive and explosive silicic eruptions. *Earth and Planetary Science Letters*, 2012, 349-350, pp.161-170. 10.1016/j.epsl.2012.06.056 . insu-00723527

HAL Id: insu-00723527

<https://insu.hal.science/insu-00723527>

Submitted on 10 Aug 2012

HAL is a multi-disciplinary open access archive for the deposit and dissemination of scientific research documents, whether they are published or not. The documents may come from teaching and research institutions in France or abroad, or from public or private research centers.

L'archive ouverte pluridisciplinaire **HAL**, est destinée au dépôt et à la diffusion de documents scientifiques de niveau recherche, publiés ou non, émanant des établissements d'enseignement et de recherche français ou étrangers, des laboratoires publics ou privés.

The effects of outgassing on the transition between effusive and explosive silicic eruptions

W. Degruyter^{a,*}, O. Bachmann^b, A. Burgisser^c, M. Manga^a

^a*Earth and Planetary Science, University of California, Berkeley, USA*

^b*Department of Earth and Space Sciences, University of Washington, Seattle, USA*

^c*Institut des Sciences de la Terre d'Orléans CNRS, Université d'Orléans, France*

Abstract

The eruption style of silicic magmas is affected by the loss of gas (outgassing) during ascent. We investigate outgassing using a numerical model for one-dimensional, two-phase, steady flow in a volcanic conduit. By implementing Forchheimer's equation rather than Darcy's equation for outgassing we are able to investigate the relative influence of Darcian and inertial permeability on the transition between effusive and explosive eruptions. These permeabilities are defined by constitutive equations obtained from textural analysis of pyroclasts and determined by bubble number density, throat-bubble size ratio, tortuosity, and roughness. The efficiency of outgassing as a function of these parameters can be quantified by two dimensionless quantities: the Stokes number, the ratio of the response time of the magma and the characteristic time of gas flow, and the Forchheimer number, the ratio of the viscous and inertial forces inside the bubble network. A small Stokes number indicates strong coupling between gas and magma and thus promotes explosive eruption. A large Forchheimer number signifies that gas escape from the bubble network is dominated by inertial effects, which leads to explosive behaviour. To provide context we compare model predictions to the May 18, 1980 Mount St. Helens and the August-September 1997 Soufrière Hills eruptions. We show that inertial effects dominate outgassing during both effusive and explosive eruptions, and that in this case the eruptive regime is determined by a new dimensionless quantity defined by the ratio of Stokes and Forchheimer number. Of the considered textural parameters, the bubble number density has the strongest influence on this quantity.

*Corresponding author

Email address: wim.degruyter@berkeley.edu (W. Degruyter)

This result has implications for permeability studies and conduit modelling.

Keywords: effusive-explosive transition, conduit, textures, permeability, outgassing

1. Introduction

The efficiency of gas escape during the ascent of silicic magma governs the transition between effusive and explosive eruptions (Slezin, 1983; Eichelberger et al., 1986; Jaupart and Allegre, 1991; Woods and Koyaguchi, 1994; Slezin, 2003; Gonnermann and Manga, 2007). If the gas can escape readily from the magma, an effusive outpouring of lava occurs. On the other hand, when the gas stays trapped within the ascending magma, it provides the potential energy needed to fragment the magma and produce an explosive eruption. Gas can separate from magma through a network of coalesced bubbles or fractures, both horizontally into the conduit walls and vertically to the surface (Stasiuk et al., 1996; Melnik and Sparks, 1999; Tuffen et al., 2003; Gonnermann and Manga, 2003). Here we study vertical gas segregation through a network of bubbles in order to quantify the effects of permeability on the outcome of an eruption.

Juvenile pyroclasts contain information on the pore-scale geometry of the magma at the time they are quenched. Pyroclasts ejected by Vulcanian eruption, for example, preserve some evidence for the effusive dome-forming phase prior to fragmentation. Formenti and Druitt (2003) found that syn-explosion bubble nucleation may occur, resulting in a uniformly distributed porosity change of $< 15\%$, which suggests that porosity trends with depth are approximately preserved in the pyroclasts. Giachetti et al. (2010) used such pyroclasts to determine pre-explosive conditions of the 1997 eruptions at Soufrière Hills Volcano, Montserrat. Products of Plinian eruptions on the other hand can record the state of the magma at fragmentation provided post-fragmentation deformation is limited. This is true for highly viscous magmas and relatively small pyroclasts. A snapshot of the outgassing history can thus be found in these pyroclasts, and measuring their permeability can provide insights into outgassing (Figure 1; Klug and Cashman, 1996; Melnik and Sparks, 2002a; Rust and Cashman, 2004; Bernard et al., 2007; Takeuchi et al., 2008; Wright et al., 2009; Bouvet de Maisonneuve et al., 2009; Yokoyama and Takeuchi, 2009).

27 It has been suggested that outgassing during magma ascent can be described by Forch-
 28 heimer’s law (Forchheimer, 1901; Rust and Cashman, 2004), an extension to Darcy’s law,
 29 which accounts for the effects of turbulence,

$$30 \quad \left| \frac{dP}{dz} \right| = \underbrace{\frac{\mu_g U}{k_1}}_{\text{viscous term}} + \underbrace{\frac{\rho_g U^2}{k_2}}_{\text{inertial term}}, \quad (1)$$

31 where z is the direction of flow, P is the pressure, U is the volume flux, μ_g is the viscosity, ρ_g is
 32 the density of the gas phase. The Darcian permeability, k_1 , and the inertial permeability, k_2 ,
 33 account for the influence of the geometry of the network of bubbles preserved in the juvenile
 34 pyroclasts. Figure 1 compiles permeability measurements as a function of the connected
 35 porosity found in pyroclasts. In general, permeability increases with increasing porosity, but
 36 there is large variability in the data sets. Effusive products are overall less porous than their
 37 explosive counterparts, but have a similar range over 5 to 6 orders of magnitude in Darcian
 38 and inertial permeability.

39 Textural studies have shown that the spread of permeability found in juvenile pyroclasts
 40 is caused by the variation in size, shape, tortuosity, and roughness of connected channels
 41 through the network of bubbles (Figure 1; Blower, 2001; Bernard et al., 2007; Wright et al.,
 42 2006, 2009; Degruyter et al., 2010a,b). Several constitutive equations that link these pa-
 43 rameters to the Darcian and inertial permeability have been proposed. In the present study
 44 we use the Kozeny-Carman or equivalent channel equations as discussed by Degruyter et al.
 45 (2010a)

$$46 \quad k_1 = \frac{r_t^2}{8} \phi_c^m, \quad (2)$$

$$48 \quad k_2 = \frac{r_t}{f_0} \phi_c^{\frac{1+3m}{2}}, \quad (3)$$

49 with ϕ_c the connected porosity, r_t the throat radius (the minimum cross section between two
 50 coalesced bubbles). The parameter m is the tortuosity or cementation factor connected to
 51 the tortuosity τ using Archie’s law,

$$52 \quad \tau^2 = \phi_c^{1-m}, \quad (4)$$

53 with the tortuosity defined as the length of the connected channels divided by the length
 54 of the porous medium. The parameter f_0 is a fitting constant that only appears in the

55 expression for k_2 , which we refer to as the roughness factor. We adapt this formulation for
56 outgassing in a conduit flow model and apply it to two well-studied eruptions: (i) the Plinian
57 phase of the May 18, 1980 eruption of Mount St. Helens, USA (MSH 1980) and (ii) the dome-
58 forming eruptions of August-September 1997 at Soufrière Hills Volcano, Montserrat (SHV
59 1997). These case studies allow us to understand the implications of using Forchheimer’s
60 equation rather than Darcy’s equation for outgassing during an eruption. We use scaling to
61 quantify the relative importance of the textural parameters and show where further under-
62 standing is needed.

63 **2. Model**

64 Conduit flow models have been successful in the past to demonstrate how gas loss de-
65 termines eruption style (Woods and Koyaguchi, 1994; Melnik and Sparks, 1999; Yoshida
66 and Koyaguchi, 1999; Slezin, 2003; Melnik et al., 2005; Kozono and Koyaguchi, 2009a,b,
67 2010). We adapt the model from Yoshida and Koyaguchi (1999) and Kozono and Koyaguchi
68 (2009a,b, 2010), which assumes a one-dimensional, steady, two-phase flow in a pipe with
69 constant radius. Relative motion between the magma (melt + crystals) and gas phase is
70 accounted for through interfacial drag forces. The exsolution of volatiles is in equilibrium
71 and the magma fragments when the gas volume fraction reaches a critical value ϕ_f . We con-
72 sider fragmentation governed by a critical strain rate (Papale, 1999) and critical overpressure
73 (Zhang, 1999); details are in Appendix B. This changes the flow from a permeable foam to
74 a gas phase with pyroclasts in suspension at which point the magma-gas friction and wall
75 friction forces are adjusted. The model of Kozono and Koyaguchi (2009a) is adapted for our
76 purpose in two ways: (i) the description of the magma rheology, and (ii) the description of
77 the interphase drag force.

78 The governing equations are:

$$79 \quad \frac{d(\rho_m u_m (1 - \phi))}{dz} = -\frac{dn}{dz} q, \quad (5)$$

$$80 \quad \frac{d(\rho_g u_g \phi)}{dz} = \frac{dn}{dz} q, \quad (6)$$

$$81 \quad \rho_m u_m (1 - \phi) \frac{du_m}{dz} = -(1 - \phi) \frac{dP}{dz} - \rho_m (1 - \phi) g + F_{mg} - F_{mw}, \quad (7)$$

$$82 \quad \rho_g u_g \phi \frac{du_g}{dz} = -\phi \frac{dP}{dz} - \rho_g \phi g - F_{mg} - F_{gw} \quad (8)$$

84 Equations (5)-(6) represent the conservation of mass and equations (7)-(8) the conservation
 85 of momentum for the magma phase (m) and the gas phase (g), where z is the vertical
 86 coordinate, u is the vertical velocity, ρ is the density, ϕ is the gas volume fraction, n is the
 87 gas mass flux fraction, q is the total mass flux, P is the pressure, F_{mg} is the magma-gas
 88 friction, and F_{mw} and F_{gw} are the wall friction with the magma and gas phase respectively.
 89 The magma is incompressible and the gas density follows the ideal gas law,

$$90 \quad \rho_g = \frac{P}{RT}, \quad (9)$$

91 where R is the specific gas constant of water and T is the temperature. Gas exsolution is
 92 governed by Henry's law for water,

$$93 \quad n = \frac{c_0 - sP^{1/2}}{1 - sP^{1/2}} \quad (n \geq 0), \quad (10)$$

94 where s is the saturation constant for water, and c_0 is the initial (dissolved) water content.

95 *2.1. Rheology*

96 The wall friction is governed by the magma phase below the fragmentation depth. As
 97 viscosity exerts a first order control on eruption dynamics, we replace the constant viscosity
 98 used in Kozono and Koyaguchi (2009a,b) by a viscosity μ_m that depends on magma properties

99 by combining models of Hess and Dingwell (1996) and Costa (2005):

$$100 \quad F_{mw} = \begin{cases} \frac{8\mu_m u_m}{r_c^2} & \phi \leq \phi_f \\ 0 & \phi > \phi_f \end{cases}, \quad (11)$$

$$101 \quad \log(\mu) = -3.545 + 0.833 \ln(100c) + \frac{9601 - 2368 \ln(100c)}{T - (195.7 + 32.25 \ln(100c))} \quad (12)$$

$$102 \quad \theta = \left\{ 1 - c_1 \operatorname{erf} \left(\frac{\sqrt{\pi}}{2} \chi \left[1 + \frac{c_2}{(1 - \chi)^{c_3}} \right] \right) \right\}^{-B/c_1} \quad (13)$$

$$103 \quad \mu_m = \mu(c, T)\theta(\chi) \quad (14)$$

105 r_c is the conduit radius, $c = sP^{1/2}$ is the dissolved water mass fraction, χ is crystal content,
 106 B is Einstein's coefficient, and c_1, c_2, c_3 are fitting coefficients. Once magma fragments we
 107 use turbulent gas-wall friction,

$$108 \quad F_{gw} = \begin{cases} 0 & \phi \leq \phi_f \\ \frac{\lambda_w}{4r_c} \rho_g |u_g| u_g & \phi > \phi_f \end{cases} \quad (15)$$

109 where λ_w is a drag coefficient.

110 2.2. Outgassing

111 Below the fragmentation depth equation (1) is implemented for the interphase drag force
 112 F_{mg} ; above the fragmentation depth we use the model in Yoshida and Koyaguchi (1999). To
 113 ease calculations before and after fragmentation there is a gradual transition region between
 114 ϕ_f and a slightly higher gas volume fraction that we define as $\phi_t = \phi_f + 0.05$.

$$115 \quad F_{mg} = \begin{cases} \left(\frac{\mu_g}{k_1} + \frac{\rho_g}{k_2} |u_g - u_m| \right) \phi (1 - \phi) (u_g - u_m) & \phi \leq \phi_f \\ \left(\frac{\mu_g}{k_1} + \frac{\rho_g}{k_2} |u_g - u_m| \right)^{1-t} \left(\frac{3C_D}{8r_a} \rho_g |u_g - u_m| \right)^t \phi (1 - \phi) (u_g - u_m) & \phi_f < \phi \leq \phi_t \\ \frac{3C_D}{8r_a} \rho_g \phi (1 - \phi) |u_g - u_m| (u_g - u_m) & \phi > \phi_t \end{cases}, \quad (16)$$

$$116 \quad t = \frac{\phi - \phi_t}{\phi_f - \phi_t},$$

118 where C_D is a drag coefficient and r_a is the average size of the fragmented magma particles.

119 To implement the Kozeny-Carman type equations (2) and (3) we have to make some further

120 assumptions about the network of bubbles:

- 121 1. Various critical porosity values for percolation have been cited in the literature (Blower,
122 2001; Burgisser and Gardner, 2004; Okumura et al., 2006; Namiki and Manga, 2008;
123 Takeuchi et al., 2009; Laumonier et al., 2011) ranging from 0.1 to 0.8 gas volume
124 fraction. Here we assume continuous percolation, i.e. the percolation threshold is
125 zero and the connected porosity is equal to the gas volume fraction ($\phi_c = \phi$). Zero
126 permeability has the same effect as very low permeability as the two phases remain
127 coupled in both cases. We note that varying the tortuosity factor is therefore equivalent
128 as varying the percolation threshold as it controls the rate at which the permeability
129 increases. A high tortuosity factor leads to a longer delay in developing permeability
130 as would a larger percolation threshold.
- 131 2. The average throat radius $r_t = f_{tb}r_b$, where f_{tb} is the throat-bubble size ratio and r_b is
132 the average bubble size.
- 133 3. The average bubble size is determined from the bubble number density and the gas
134 volume fraction as in Gonnermann and Manga (2005),

$$135 \quad r_b = \left(\frac{\phi}{\frac{4\pi}{3}N_d(1-\phi)} \right)^{1/3}. \quad (17)$$

136 These assumptions bring us to the following closure equations for the permeability

$$137 \quad k_1 = \frac{(f_{tb}r_b)^2}{8}\phi^m, \quad (18)$$

$$138 \quad k_2 = \frac{(f_{tb}r_b)}{f_0}\phi^{\frac{1+3m}{2}}. \quad (19)$$

139

140 Bounds on the four parameters can be found in the literature: $N_d = 10^8-10^{16} \text{ m}^{-3}$ (Klug and
141 Cashman, 1994; Polacci et al., 2006; Sable et al., 2006; Giachetti et al., 2010), $f_{tb} = 0.1 - 1$
142 (Saar and Manga, 1999; Degruyter et al., 2010a), $m = 1 - 10$ (Le Pennec et al., 2001;
143 Bernard et al., 2007; Wright et al., 2009; Degruyter et al., 2010a,b), and Degruyter et al.
144 (2010a) estimated f_0 between 10 and 100 for pumices. For comparison, f_0 for permeameter
145 standards used by Rust and Cashman (2004) is estimated to be around 0.025 and for packed
146 beds a value of 1.75 is found (Ergun, 1952).

147 The set of equations (5)-(19) can be converted into two ordinary differential equations
148 for P and ϕ . We set the differential velocity between the two phases to be initially zero.

149 In combination with two boundary conditions: (i) initial pressure P_0 , and (ii) atmospheric
 150 pressure or the choking condition at the vent, this 2-point boundary value problem is solved
 151 using the ordinary differential equation solver *ode23s* built in Matlab (Shampine and Re-
 152 ichelt, 1997) in combination with a shooting method. Table 1 summarizes model parameters
 153 used in this study.

154 The behaviour of this model allows us to distinguish between explosive and effusive
 155 eruptions. Figure 2 shows profiles of pressure, gas volume fraction, velocity, and permeability
 156 for a representative explosive and effusive case. In the explosive case the pressure rapidly
 157 decreases just prior to fragmentation, while in the effusive case the pressure remains close
 158 to magmastatic (Figure 2a). The gas volume fraction reaches high values in the case of an
 159 explosive eruption, while in the effusive case it reaches a maximum and decreases at low
 160 pressures (Figure 2b). The velocity of the gas phase starts to differ from that of the magma
 161 phase at depth in the case of an effusive eruption, while in the explosive case velocities of
 162 both phases are nearly equal until fragmentation after which they start to differ (Figure
 163 2c). Both Darcian and inertial permeability are larger at similar pressures in the case of an
 164 effusive eruption compared to the explosive case (Figure 2d).

165 3. Stokes and Forchheimer number

166 We focus on the influence of the textural parameters N_d , f_{tb} , m , and f_0 on the eruption
 167 style. We therefore non-dimensionalize the equations (5)-(19) using initial and boundary
 168 conditions as reference values to extract dimensionless quantities that depend on textures
 169 (see Appendix A for details). These are found to be the Stokes number, St , and the
 170 Forchheimer number, Fo . St is the ratio of the response time scale of the magma and the
 171 characteristic flow time of the gas phase

$$172 \quad St = \frac{\tau_V}{\tau_F} = \frac{\rho_m k_{10}}{\frac{\mu_g}{U_0}} \quad (20)$$

173 with U_0 and k_{10} the reference velocity and Darcian permeability respectively (Appendix A).
 174 When St is small the magma and gas phase are closely coupled and ascend at the same
 175 speed, while for a large St the gas decouples from the magma and can ascend more rapidly

176 than the magma. Fo is the ratio of the inertial term and the viscous term in Forchheimer's
177 equation

$$178 \quad \text{Fo} = \frac{\rho_{g0} k_{10} U_0}{k_{20} \mu_g}. \quad (21)$$

179 with ρ_{g0} and k_{20} the reference gas density and inertial permeability respectively (Appendix
180 A). For a low Fo the outgassing is controlled by the Darcian permeability, while for a high
181 Fo the inertial permeability is dominant. We are now able to explore the effusive-explosive
182 transition in terms of St and Fo when conduit geometry and magma properties are held
183 constant. In other words, by looking at specific eruptions we can single out the influence of
184 textures from other parameters. This strategy is used in the following section. Monte Carlo
185 simulations are used to explore the texture parameter space defined by N_d , f_{tb} , m , and f_0 .
186 We determine if the eruption is explosive or effusive for each combination of parameters and
187 then map the results on the (St,Fo)-space.

188 4. Results

189 4.1. Mount St. Helens May 18, 1980 eruption

190 The MSH 1980 eruption is a good case study of an explosive eruption as extensive data has
191 been collected on magma properties, conduit geometry, and textures. We use the magma
192 properties as obtained by Blundy and Cashman (2005) and listed in Table 1. Following
193 Dobran (1992) the conduit length was estimated from lithostatic pressure $P_0/\rho g = 5291$ m
194 for a wall rock density of 2700 kg/m^3 . The fragmentation criterion is set by a critical gas
195 volume fraction ϕ_f at 0.8 as found in the white pumice produced by this eruption (Klug
196 and Cashman, 1994). We use a conduit radius of $r_c = 30$ m to match the mass flow rates
197 estimated by Carey et al. (1990). Figure 2 shows the typical behaviour of an explosive
198 eruption for these conditions.

199 The results of the Monte Carlo simulations over the texture parameter space are divided
200 into explosive and effusive eruptions and projected on a (St,Fo)-map (Figure 3). Parameters
201 leading to explosive eruptions occupy a region of the (St,Fo)-space separated from the ones of
202 leading to effusive eruptions. The separation between these two regions can be approximated
203 by a linear relationship defined by a critical Stokes number St_c and critical Forchheimer

204 number Fo_c ,

$$205 \quad Fo = \frac{Fo_c}{St_c}(St - St_c). \quad (22)$$

206 Such a relationship can be expected when inspecting equation (A.14) that shows that the
207 dimensionless drag is inversely correlated with St and linearly with Fo . For MSH 1980
208 conditions we found $St_c \approx 10^{-3}$ and $Fo_c \approx 50$.

209 The definition of St and Fo in combination with the effusive-explosive map can now be
210 used to interpret the influence of each of the textural parameters individually (Figure 3a).
211 Starting from an arbitrarily chosen point on the (St, Fo) map, we increase the value of one of
212 the textural parameters, while keeping the others constant. Increasing the bubble number
213 density N_d leads to higher coupling between gas and magma, while turbulent outgassing
214 becomes less dominant. This results in conditions favorable for explosive eruptions. The
215 opposite effect is noted for the throat-bubble ratio f_{tb} . An increase of the tortuosity factor
216 m leads to increased coupling between the gas and magma as well as increased dominance of
217 turbulent outgassing, which makes explosive eruptions more likely. Increasing the roughness
218 factor f_0 increases Fo and leaves St constant. This brings conditions closer to the explosive
219 regime where outgassing is governed by the inertial term in equation (1). The size of the
220 arrows is based on the variability of each of the parameters found in the literature. The
221 large range in measurements of bubble number density implies that this is the main textural
222 feature that controls outgassing. The influence of other parameters is smaller, but we note
223 that uncertainty can be large, especially in the case of the roughness factor f_0 for which data
224 are sparse.

225 The textural studies by Klug and Cashman (1994, 1996) provide constraints on where
226 the MSH 1980 eruption falls on this regime diagram (Figure 3b). A bubble number density
227 of $N_d = 10^{15} \text{ m}^{-3}$ and tortuosity factor of $m = 3.5$ was measured. The St and Fo number
228 range for the MSH 1980 eruption (Figure 3b) predict a permeability between $5 \times 10^{-14} \text{ m}^2$
229 and $5 \times 10^{-12} \text{ m}^2$ near fragmentation in agreement with the data of Klug and Cashman
230 (1996). The failure of the bubbles to form larger connected channels does not allow for
231 the gas to decouple from the magma and an explosive eruption results ($St < St_c$). The
232 spread for the roughness factor f_0 puts the MSH 1980 eruption in the turbulent outgassing

233 regime ($Fo > Fo_c$), implying that the outgassing was dominated by the inertial permeability.
234 Measurements of inertial permeability on MSH 1980 pyroclasts could test this hypothesis.

235 The use of a critical gas volume fraction as a criterion for fragmentation has been shown
236 to be oversimplified and a stress-based criterion either by critical strain rate or gas overpres-
237 sure is now favored (Dingwell, 1996; Papale, 1999; Zhang, 1999). However, using different
238 fragmentation mechanisms in a one-dimensional conduit model leads to qualitatively similar
239 results as the runaway effect that leads to increased acceleration will ensure all fragmenta-
240 tion criteria will be met over the same narrow depth interval (Melnik and Sparks, 2002b;
241 Massol and Koyaguchi, 2005). In other words, a critical gas volume fraction has similar
242 consequences as a critical strain rate or overpressure in this type of model. This effect is
243 demonstrated here using a criterion based on strain rate and one on overpressure (Appendix
244 B). The strain rate criterion leads to explosive eruptions at a gas volume fraction of about
245 0.85, while the overpressure criterion was equivalent to a gas volume fraction near 0.6. This
246 leads to a shift in the critical Stokes number defining the transition curve, while its shape
247 is preserved (Figure 3b). We have chosen the critical gas volume fraction that matches the
248 observations in the pyroclasts of the MSH 1980 and note that this is equivalent to the choice
249 of a critical stress criterion.

250 The calculated mass flow rates vary little within each of the eruption regimes, showing
251 that textural parameters have little influence on it. Rather, mass flow rate appears domi-
252 nantly controlled by the magma properties and conduit geometry in combination with the
253 imposed boundary conditions at the top and bottom of the conduit. In the explosive regime
254 the mass flow rate is limited by the choked flow condition at the vent and the conduit ra-
255 dius. For the MSH 1980 conditions we obtain 2×10^7 kg/s by setting the conduit radius
256 to match the mass flow rate estimates of Carey et al. (1990). In the effusive regime the
257 top boundary condition becomes the ambient pressure and mass flow rates are controlled
258 mostly by magma viscosity and conduit radius (Melnik et al., 2005; Kozono and Koyaguchi,
259 2009a,b). For the MSH 1980 conditions we find a mass flow rate around 2×10^6 kg/s, an
260 order of magnitude smaller than in the explosive case. The lava dome growth that followed
261 the MSH 1980 eruption had mass flow rates around $1 - 5 \times 10^4$ kg/s (Moore et al., 1981).

262 This large mismatch implies that the rheology and/or geometry during the dome-forming
 263 eruption significantly changed from the explosive MSH 1980 eruption. These issues could
 264 be addressed by incorporating improved rheology laws (Cordonnier et al., 2009) as well as
 265 crystallization kinetics (Blundy and Cashman, 2005; Melnik et al., 2011) into the model.
 266 However, we can conclude that bubble number density, throat-bubble size ratio, tortuosity,
 267 and roughness factor play a secondary role in controlling the mass flow rate.

268 *4.2. August-September 1997 Soufrière Hills Volcano dome-forming eruptions*

269 The SHV 1997 dome-forming eruptions provide a well-defined case study for an effusive
 270 eruption. Note that we use our model only for the dome-forming phase and not for the
 271 Vulcanian eruptions, which require a model that contains transient dynamics (Melnik and
 272 Sparks, 2002b; de' Michieli Vitturi et al., 2010; Fowler et al., 2010). We used the eruption
 273 conditions summarized by Melnik and Sparks (1999) and Clarke et al. (2007): a temperature
 274 of 1123 K, conduit length of 5 km, initial pressure of 120 MPa, volatile content of 4.6 wt.%
 275 water, and magma density of 2450 kg/m³. As was evident from the simulations under MSH
 276 1980 eruption conditions, in the case of effusive eruptions crystallization due to decompres-
 277 sion needs to be taken into account in order to capture the lower mass flow rates. We adopt
 278 the parametrization as formulated by de' Michieli Vitturi et al. (2010) based on the work of
 279 Couch et al. (2003) for the relationship between χ and P

$$280 \quad \chi = \min \left[\chi_{\max}, \chi_0 + 0.55 \left(0.58815 \left(\frac{P}{10^6} \right)^{-0.5226} \right) \right] \quad (23)$$

281 where $\chi_{\max} = 0.6$ and the initial crystal volume fraction is 0.45. Setting the conduit radius
 282 at $r_c = 22.5$ m gives a mass flow rate of 3.5×10^4 kg/s in the effusive regime, in agreement
 283 with Druitt et al. (2002). Figure 2 shows example (effusive) profiles produced for these
 284 conditions. The mass flow rate in the explosive regime under SHV 1997 conditions is higher
 285 by nearly two orders of magnitude, 2.2×10^6 kg/s. We stress that this is not related to
 286 the mass flow rate associated to the Vulcanian explosions at Soufrière Hills Volcano as we
 287 only model steady state eruptions, which are dynamically very different from the Vulcanian
 288 eruptions (Melnik and Sparks, 2002b; de' Michieli Vitturi et al., 2010; Fowler et al., 2010).

289 Using again the strategy of Monte Carlo simulations over the textural parameter space,
 290 we obtain a new (St,Fo)-map for SHV 1997 conditions that is split into an effusive and
 291 explosive region by a transition curve approximated by equation (22) with $St_c = 2.5 \times 10^{-5}$
 292 and $Fo_c = 100$. There is a strong shift of the transition curve compared to MSH 1980 with
 293 St_c about two orders of magnitude smaller. This is due to the two orders of magnitude
 294 increase of the effective viscosity controlled by the increase in crystal content during ascent.
 295 A parameter that is highly uncertain is the critical condition for explosive eruption, as we
 296 cannot interpret pyroclast vesicularity of the SHV 1997 eruption in the same fashion as the
 297 quenched samples from MSH 1980 eruption. We have chosen $\phi_f = 0.8$.

298 The bubble number density of the SHV 1997 eruptions during the dome-forming stage is
 299 between 10^9 and 10^{10} m^{-3} , based on the large-bubble population in the pyroclasts produced
 300 by the Vulcanian eruptions (Giachetti et al., 2010). The St-Fo region defined by this number
 301 is indicated in black on Figure 4a. This region can be refined by using the relationship
 302 between pressure and gas volume fraction in the conduit as reconstructed by Clarke et al.
 303 (2007) and Burgisser et al. (2010). Using Monte Carlo simulations we can search for the
 304 St-Fo values that best fit this profile. There is a large spread of the data near the top of the
 305 conduit ($< 10 \text{ MPa}$) indicating a complex and non-unique behaviour in the conduit plug in
 306 between Vulcanian eruptions (de' Michieli Vitturi et al., 2010). Therefore we fit the model to
 307 the data at greater depth ($> 10 \text{ MPa}$). The best fit as determined by the lowest chi-square
 308 value was $St = 2.6 \times 10^{-1}$, $Fo = 3.7 \times 10^4$, which can be formed by e.g. $N_d = 10^{9.5} \text{ m}^{-3}$,
 309 $f_{tb} = 10^{-0.5}$, $m = 2.1$, and $f_0 = 10$ (Figure 4b). Below the conduit plug, bubbles create
 310 large enough pathways through the magma to allow gas escape at low gas volume fraction,
 311 thereby hindering magma acceleration ($St > St_c$). Figure 4b indicates, as in the case of MSH
 312 1980, that outgassing is turbulent ($Fo > Fo_c$) and dominated by inertial permeability.

313 4.3. Influence of turbulent outgassing on the effusive-explosive transition

314 The transition curve separating the effusive and explosive eruption regimes in terms of
 315 textures is determined by a critical Stokes and Forchheimer number, the values of which will

316 depend on magma properties and conduit geometry, i.e.

$$317 \quad \text{St}_c = \Phi_1 (\text{Re}, \text{Fr}, \text{Ma}, c_0, \chi_0, \phi_f, \delta, \sigma, a_r), \quad (24)$$

$$318 \quad \text{Fo}_c = \Phi_2 (\text{Re}, \text{Fr}, \text{Ma}, c_0, \chi_0, \phi_f, \delta, \sigma, a_r). \quad (25)$$

319

320 Regardless of the exact forms of these equations, the results show a change in the eruption
 321 dynamics when changing from laminar ($\text{Fo} \ll \text{Fo}_c$) to turbulent outgassing ($\text{Fo} \gg \text{Fo}_c$). This
 322 becomes more clear when we inspect equation (22) and rewrite it as

$$323 \quad \text{St} = \text{St}_c \left(1 + \frac{\text{Fo}}{\text{Fo}_c} \right). \quad (26)$$

324 We see that in the case of laminar outgassing ($\text{Fo} \ll \text{Fo}_c$) the transition is simply described
 325 by $\text{St} \approx \text{St}_c$. In the case of turbulent outgassing ($\text{Fo} \gg \text{Fo}_c$) the transition occurs when

$$326 \quad \Pi = \frac{\text{St}}{\text{Fo}} = \frac{\rho_m k_{20}}{\rho_{g0} r_c} \approx \Pi_c = \frac{\text{St}_c}{\text{Fo}_c}, \quad (27)$$

327 with Π a new dimensionless quantity defined as the ratio of the St and Fo . Textural mea-
 328 surements on juvenile pyroclasts in combination with our numerical results suggest that Fo
 329 $\gg \text{Fo}_c$ (Figures 3b and 4b) and thus that Π is the relevant quantity for the effusive-explosive
 330 transition rather than St . Equation (27) reveals that the variation of Π is mostly due to
 331 the ratio of the characteristic inertial permeability with respect to the conduit radius as
 332 the density ratio between the magma and the gas will not vary much over a wide range of
 333 parameters. Hence, in order to have an effusive eruption the inertial permeability that has
 334 to develop during a volcanic eruption needs to be higher in a conduit with a large radius
 335 than one with a small radius. In other words, a conduit with a large radius is more likely to
 336 produce an explosive eruption.

337 5. Concluding remarks

338 We developed a model to study the effect of outgassing on eruption style with a specific
 339 focus on the effect of using Forchheimer's equation instead of Darcy's equation. We suggest
 340 that the inertial term in Forchheimer's equation is dominant during both explosive and ef-
 341 fusive eruptions. In terms of textural parameters, the radius of connected channels through

342 the bubble network dominates the outgassing dynamics. The channel radii are controlled
343 by bubble number density and throat-bubble size ratio, and can vary over many orders of
344 magnitude. Higher tortuosity and roughness factor increase the chances for an explosive
345 eruption, but are less important. However, attention needs to be drawn towards the rough-
346 ness factor as it is the least constrained parameter. Even if the roughness factor would be
347 lowered by several orders of magnitude, the estimated Fo for MSH 1980 and SHV 1997 would
348 still be above Fo_c . In terms of dimensionless parameters this means that the shift in erup-
349 tion style is not governed by St as previously assumed (e.g., Melnik et al., 2005; Kozono and
350 Koyaguchi, 2009a,b) but by Π as defined in equation (27). This result has implications for
351 (i) permeability studies on juvenile pyroclasts that need to quantify the controls on inertial
352 permeability (Rust and Cashman, 2004; Mueller et al., 2005; Takeuchi et al., 2008; Bouvet de
353 Maisonneuve et al., 2009; Yokoyama and Takeuchi, 2009; Degruyter et al., 2010a) and (ii)
354 conduit models that need to include the inertial term in the closure equation for outgassing
355 (Fowler et al., 2010).

356 Products from effusive eruptions tend to have a lower porosity than their explosive coun-
357 terparts, while their permeability can reach similar high values (Figure 1). Although pyro-
358 clasts of effusive eruptions can be altered by bubble expansion after dome collapse or bubble
359 collapse during emplacement, the porosity-permeability measurements in combination with
360 the conduit model show that high permeability at low porosity can be explained by a larger
361 radius of permeable channels. Such channels can develop due to low bubble number density
362 (Giachetti et al., 2010) and early coalescence due to pre-eruptive magma heating (Ruprecht
363 and Bachmann, 2010) or deformation (Okumura et al., 2006; Laumonier et al., 2011). Hys-
364 teresis, whereby high permeability is preserved and porosity is decreased by bubble collapse,
365 can further enhance the difference between effusive and explosive products (Saar and Manga,
366 1999; Rust and Cashman, 2004; Michaut et al., 2009).

367 Several additions to the model can be made to improve quantification of the effusive-
368 explosive transition. The most important include adding spatial (Dufek and Bergantz, 2005)
369 and temporal variations (Melnik and Sparks, 2002b; de' Michieli Vitturi et al., 2010; Fowler
370 et al., 2010) as well as non-equilibrium growth of bubbles (Burgisser and Gardner, 2004;

371 Gonnermann and Manga, 2005) and crystals (Melnik et al., 2011). In explosive eruptions,
372 delayed bubble growth will reduce development of permeability and crystals will not be
373 able to grow fast enough to increase viscosity and reduce the ascent speed. On the other
374 hand, in effusive eruptions both bubble and crystal growth will be closer to equilibrium.
375 Including spatial and temporal variation will help identify the development of heterogeneity
376 of permeability inside the conduit.

377 By treating the textural properties independent from magma properties and conduit ge-
378 ometry we were able to distill the relative importance of these properties on outgassing.
379 However, textures are intimately tied to the magma properties as they control nucleation,
380 growth, deformation and coalescence of bubbles. For example, bubble number density will in-
381 crease with increasing decompression rate (Toramaru, 2006) and decrease due to coalescence
382 (Burgisser and Gardner, 2004), while tortuosity can be lowered by deformation (Degruyter
383 et al., 2010a). Incorporating the coupling between the textures and the magma properties
384 is worthy of future study.

385 **Acknowledgments**

386 WD was supported by the Swiss National Science Foundation Grant No. PBGEP2-
387 131251, and MM by NSF EAR 1049662. We thank Sebastian Mueller for providing perme-
388 ability data and two reviewers for their comments that improved this paper.

389 **References**

- 390 Bernard, M.L., Zamora, M., Geraud, Y., Boudon, G., 2007. Transport properties of pyro-
391 clastic rocks from Montagne Pelée volcano (Martinique, Lesser Antilles). *J. Geophys. Res.*
392 112, B05205. doi:10.1029/2006JB004385.
- 393 Blower, J.D., 2001. Factors controlling permeability-porosity relationships in magma. *Bull.*
394 *Volcanol.* 63, 497–504. doi:10.1007/s004450100172.
- 395 Blundy, J., Cashman, K., 2005. Rapid decompression-driven crystallization recorded by melt
396 inclusions from Mount St. Helens volcano. *Geology* 33, 793–796. doi:10.1130/G21668.1.

- 397 Burgisser, A., Gardner, J.E., 2004. Experimental constraints on degassing and permeability
398 in volcanic conduit flow. *Bull. Volcanol.* 67, 42–56. doi:10.1007/s00445-004-0359-5.
- 399 Burgisser, A., Poussineau, S., Arbaret, L., Druitt, T., Giachetti, T., Bourdier, J.L., 2010.
400 Pre-explosive conduit conditions of the 1997 Vulcanian explosions at Soufrière Hills Vol-
401 cano, Montserrat: I. pressure and vesicularity distributions. *J. Volcanol. Geotherm. Res.*
402 194, 27–41. doi:10.1016/j.jvolgeores.2010.04.008.
- 403 Carey, S., Sigurdsson, H., Gardner, J., Criswell, W., 1990. Variations in column height and
404 magma discharge during the May 18, 1980 eruption of Mount St. Helens. *J. Volcanol.*
405 *Geotherm. Res.* 43, 99–112. doi:10.1016/0377-0273(90)90047-J.
- 406 Clarke, A., Stephens, S., Teasdale, R., Sparks, R., Diller, K., 2007. Petrologic con-
407 straints on the decompression history of magma prior to Vulcanian explosions at
408 the Soufrière Hills volcano, Montserrat. *J. Volcanol. Geotherm. Res.* 161, 261–274.
409 doi:10.1016/j.jvolgeores.2006.11.007.
- 410 Cordonnier, B., Hess, K.U., Lavalley, Y., Dingwell, D.B., 2009. Rheological properties
411 of dome lavas: Case study of Unzen volcano. *Earth Planet. Sci. Lett.* 279, 263–272.
412 doi:10.1016/j.epsl.2009.01.014.
- 413 Costa, A., 2005. Viscosity of high crystal content melts: dependence on solid fraction.
414 *Geophys. Res. Lett.* 32, L22308. doi:10.1029/2005GL024303.
- 415 Couch, S., Sparks, R., Carroll, M., 2003. The kinetics of degassing-induced crys-
416 tallization at Soufrière Hills Volcano, Montserrat. *J. Petrol.* 44, 1477–1502.
417 doi:10.1093/petrology/44.8.1477.
- 418 Degruyter, W., Bachmann, O., Burgisser, A., 2010a. Controls on magma permeability in
419 the volcanic conduit during the climactic phase of the Kos Plateau Tuff eruption (Aegean
420 Arc). *Bull. Volcanol.* 72, 63–74. doi:10.1007/s00445-009-0302-x.
- 421 Degruyter, W., Burgisser, A., Bachmann, O., Malaspinas, O., 2010b. Synchrotron X-ray

422 microtomography and lattice Boltzmann simulations of gas flow through volcanic pumices.
423 *Geosphere* 6, 470–481. doi:10.1130/GES00555.1.

424 Dingwell, D.B., 1996. Volcanic dilemma: Flow or blow? *Science* 273, 1054–1055.
425 doi:10.1126/science.273.5278.1054.

426 Dobran, F., 1992. Nonequilibrium flow in volcanic conduits and application to the eruptions
427 of Mt. St. Helens on May 18, 1980, and Vesuvius in AD 79. *J. Volcanol. Geotherm. Res.*
428 49, 285–311. doi:10.1016/0377-0273(92)90019-A.

429 Druitt, T., Young, S., Baptie, B., Bonadonna, C., Calder, E., Clarke, A., Cole, P., Harford,
430 C., Herd, R., Luckett, R., Ryan, G., Voight, B., 2002. Episodes of cyclic vulcanian
431 explosive activity with fountain collapse at Soufriere Hills Volcano, Montserrat, in: Druitt,
432 T., Kokelaar, B. (Eds.), *The eruption of Soufriere Hills Volcano, Montserrat, from 1995 to*
433 *1999*, The Geological Society of London. pp. 281–306.

434 Dufek, J., Bergantz, G.W., 2005. Transient two-dimensional dynamics in the upper conduit
435 of a rhyolitic eruption: A comparison of closure models for the granular stress. *J. Volcanol.*
436 *Geotherm. Res.* 143, 113–132. doi:10.1016/j.jvolgeores.2004.09.013.

437 Eichelberger, J., Carrigan, C., Westrich, H., Price, R., 1986. Non-explosive silicic volcanism.
438 *Nature* 323, 598–602. doi:10.1038/323598a0.

439 Ergun, S., 1952. Fluid flow through packed columns. *Chem. Eng. Prog.* 46, 89–94.

440 Forchheimer, P., 1901. Wasserbewegung durch boden. *Z. Ver. Dtsch. Ing.* 45, 1782–1788.

441 Formenti, Y., Druitt, T.H., 2003. Vesicle connectivity in pyroclasts and implications for the
442 fluidization of fountain-collapse pyroclastic flows, Montserrat (West Indies). *Earth Planet.*
443 *Sci. Lett.* 214, 561–574. doi:10.1016/S0012-821X(03)00386-8.

444 Fowler, A.C. Scheu, B., Lee, W., McGuinness, M., 2010. A theoretical model of
445 the explosive fragmentation of vesicular magma. *Proc. R. Soc. A* 466, 731–752. doi:
446 10.1098/rspa.2009.0382.

- 447 Giachetti, T., Druitt, T., Burgisser, A., Arbaret, L., Galven, C., 2010. Bub-
448 ble nucleation, growth and coalescence during the 1997 Vulcanian explosions of
449 Soufrière Hills Volcano, Montserrat. *J. Volcanol. Geotherm. Res.* 193, 215–231.
450 doi:10.1016/j.jvolgeores.2010.04.001.
- 451 Gonnermann, H.M., Manga, M., 2003. Explosive volcanism may not be an inevitable con-
452 sequence of magma fragmentation. *Nature* 426, 432–435. doi:10.1038/nature02138.
- 453 Gonnermann, H.M., Manga, M., 2005. Nonequilibrium magma degassing: Results from
454 modeling of the ca. 1340 A.D. eruption of Mono Craters, California. *Earth Planet. Sci.*
455 *Lett.* 238, 1–16. doi:10.1016/j.epsl.2005.07.021.
- 456 Gonnermann, H.M., Manga, M., 2007. The fluid mechanics inside a volcano. *Annu. Rev.*
457 *Fluid Mech.* 39, 321–356. doi:10.1146/annurev.fluid.39.050905.110207.
- 458 Hess, K., Dingwell, D., 1996. Viscosities of hydrous leucogranitic melts: a non-Arrhenian
459 model. *Am. Mineral.* 81, 1297–1300.
- 460 Jaupart, C., Allegre, C., 1991. Gas content, eruption rate and instabilities of eruption
461 regime in silicic volcanoes. *Earth Planet. Sci. Lett.* 102, 413–429. doi:10.1016/0012-
462 821X(91)90032-D.
- 463 Klug, C., Cashman, K.V., 1994. Vesiculation of May 18, 1980 Mount St. Helens magma.
464 *Geology* 22, 468–472. doi:10.1130/0091-7613(1994)022;0468:VOMMSH;2.3.CO;2.
- 465 Klug, C., Cashman, K.V., 1996. Permeability development in vesiculating magmas: Impli-
466 cations for fragmentation. *Bull. Volcanol.* 58, 87–100. doi:10.1007/s004450050128.
- 467 Kozono, T., Koyaguchi, T., 2009a. Effects of relative motion between gas and liquid on 1-
468 dimensional steady flow in silicic volcanic conduits: 1. an analytical method. *J. Volcanol.*
469 *Geotherm. Res.* 180, 21–36. doi:10.1016/j.jvolgeores.2008.11.006.
- 470 Kozono, T., Koyaguchi, T., 2009b. Effects of relative motion between gas and liquid on
471 1-dimensional steady flow in silicic volcanic conduits: 2. origin of diversity of eruption
472 styles. *J. Volcanol. Geotherm. Res.* 180, 37–49. doi:10.1016/j.jvolgeores.2008.11.007.

- 473 Kozono, T., Koyaguchi, T., 2010. A simple formula for calculating porosity of magma
474 in volcanic conduits during dome-forming eruptions. *Earth Planets Space* 62, 483–488.
475 doi:10.5047/eps.2010.02.005.
- 476 Laumonier, M., Arbaret, L., Burgisser, A., Champallier, R., 2011. Porosity redistribu-
477 tion enhanced by strain localization in crystal-rich magmas. *Geology* 39, 715–718.
478 doi:10.1130/G31803.1.
- 479 Le Pennec, J.L., Hermitte, D., Dana, I., Pezard, P., Coulon, C., Cocheme, J.J., Mulyadi, E.,
480 Ollagnier, F., Revest, C., 2001. Electrical conductivity and pore-space topology of Merapi
481 lavas: Implications for the degassing of porphyritic andesite magmas. *Geophys. Res. Lett.*
482 28, 4283–4286. doi:10.1029/2001GL013401.
- 483 Bouvet de Maisonneuve, C., Bachmann, O., Burgisser, A., 2009. Characterization of juvenile
484 pyroclasts from the Kos Plateau Tuff (Aegean Arc): insights into the eruptive dynamics
485 of a rhyolitic caldera-forming eruption. *Bull. Volcanol.* 71, 643–658. doi:10.1007/s00445–
486 008–0250–x.
- 487 Massol, H., Koyaguchi, T., 2005. The effect of magma flow on nucleation of
488 gas bubbles in a volcanic conduit. *J. Volcanol. Geotherm. Res.* 143, 69–88.
489 doi:10.1016/j.jvolgeores.2004.09.011.
- 490 Melnik, O., Barmin, A.A., Sparks, R.S.J., 2005. Dynamics of magma flow inside volcanic
491 conduits with bubble overpressure buildup and gas loss through permeable magma. *J.*
492 *Volcanol. Geotherm. Res.* 143, 53–68. doi:10.1016/j.jvolgeores.2004.09.010.
- 493 Melnik, O., Sparks, R., 1999. Nonlinear dynamics of lava dome extrusion. *Nature* 402,
494 37–41. doi:10.1038/46950.
- 495 Melnik, O., Sparks, R.S.J., 2002a. Dynamics of magma ascent and lava extrusion at Soufrière
496 Hills Volcano, Montserrat, in: Druitt, T., Kokelaar, B. (Eds.), *The eruption of Soufrière*
497 *Hills Volcano, Montserrat, from 1995 to 1999*, The Geological Society of London. pp.
498 153–171.

- 499 Melnik, O., Sparks, R.S.J., 2002b. Modelling of conduit flow dynamics during explosive
500 activity at Soufriere Hills Volcano, Montserrat, in: Druitt, T., Kokelaar, B. (Eds.), The
501 eruption of Soufriere Hills Volcano, Montserrat, from 1995 to 1999, The Geological Society
502 of London. pp. 307–317.
- 503 Melnik, O.E., Blundy, J.D., Rust, A., Muir, D.D., 2011. Subvolcanic plumbing systems
504 imaged through crystal size distributions. *Geology* 39, 403406. doi:10.1130/G31691.1.
- 505 Michaut, C., Bercovici, D., Sparks, R.S.J., 2009. Ascent and compaction of gas rich
506 magma and the effects of hysteretic permeability. *Earth Planet. Sci. Lett.* 282, 258–267.
507 doi:10.1016/j.epsl.2009.03.026.
- 508 de' Michieli Vitturi, M., Clarke, A., Neri, A., Voight, B., 2010. Transient effects of magma
509 ascent dynamics along a geometrically variable dome-feeding conduit. *Earth Planet. Sci.*
510 *Lett.* 295, 541–553. doi:10.1016/j.epsl.2010.04.029.
- 511 Moore, J., Lipman, P., Swanson, D., Alpha, T.R., 1981. Growth of lava domes in the crater,
512 June 1980-January 1981, in: Lipman, P.W. and Mullineaux, D. (Ed.), The 1980 eruptions
513 of Mount St. Helens, Washington, US Gov. Printing Office, Washington, DC, USA. pp.
514 541–547.
- 515 Mueller, S., Melnik, O., Spieler, O., Scheu, B., Dingwell, D.B., 2005. Permeability and
516 degassing of dome lavas undergoing rapid decompression: An experimental determination.
517 *Bull. Volcanol.* 67, 526–538. doi:10.1007/s00445-004-0392-4.
- 518 Namiki, A., Manga, M., 2008. Transition between fragmentation and permeable
519 outgassing of low viscosity magmas. *J. Volcanol. Geotherm. Res.* 169, 48–60.
520 doi:10.1016/j.jvolgeores.2007.07.020.
- 521 Okumura, S., Nakamura, M., Tsuchiyama, A., 2006. Shear-induced bubble coales-
522 cence in rhyolitic melts with low vesicularity. *Geophys. Res. Lett.* 33, L20316,
523 doi:10.1029/2006GL027347.

- 524 Papale, P., 1999. Strain-induced magma fragmentation in explosive eruptions. *Nature* 397,
525 425–428. doi:10.1038/17109.
- 526 Polacci, M., Baker, D.R., Mancini, L., Tromba, G., Zanini, F., 2006. Three-dimensional
527 investigation of volcanic textures by X-ray microtomography and implications for conduit
528 processes. *Geophys. Res. Lett.* 33, L13312. doi:10.1029/2006GL026241.
- 529 Ruprecht, P., Bachmann, O., 2010. Pre-eruptive reheating during magma mixing at Quizapu
530 volcano and the implications for the explosiveness of silicic arc volcanoes. *Geology* 38, 919–
531 922. doi:10.1130/G31110.1.
- 532 Rust, A.C., Cashman, K.V., 2004. Permeability of vesicular silicic magma: inertial and
533 hysteresis effects. *Earth Planet. Sci. Lett.* 228, 93–107. doi:10.1016/j.epsl.2004.09.025.
- 534 Saar, M.O., Manga, M., 1999. Permeability-porosity relationship in vesicular basalts. *Geo-*
535 *phys. Res. Lett.* 26, 111–114. doi:10.1029/1998GL900256.
- 536 Sable, J., Houghton, B., Del Carlo, P., Coltelli, M., 2006. Changing conditions of magma
537 ascent and fragmentation during the Etna 122 BC basaltic Plinian eruption: Evidence from
538 clast microtextures. *Bull. Volcanol.* 158, 333–354. doi:10.1016/j.jvolgeores.2006.07.006.
- 539 Shampine, L.F., Reichelt, M.W., 1997. The Matlab ODE suite. *SIAM J. Sci. Stat. Comp.*
540 18, 1–22. doi:10.1137/S1064827594276424.
- 541 Slezin, Y.B., 1983. The dynamics of dispersion regime in volcanic eruptions: 1. Theoretical
542 description of magma movement through volcanic conduit (in Russian). *Vulkanol Sejsmol*
543 5, 9–17.
- 544 Slezin, Y.B., 2003. The mechanism of volcanic eruptions (a steady state approach). *J.*
545 *Volcanol. Geotherm. Res.* 122, 7–50. doi:10.1016/S0377-0273(02)00464-X.
- 546 Stasiuk, M., Barclay, J., Carroll, M., Jaupart, C., Ratt, J., Sparks, R., Tait, S., 1996. De-
547 gassing during magma ascent in the Mule Creek vent (USA). *Bull. Volcanol.* 58, 117–130.
548 doi:10.1007/s004450050130.

- 549 Takeuchi, S., Nakashima, S., Akihiko Tomiya, A., 2008. Permeability measurements of
550 natural and experimental volcanic materials with a simple permeameter: Toward an un-
551 derstanding of magmatic degassing processes. *J. Volcanol. Geotherm. Res.* 177, 329–339.
552 doi:10.1016/j.jvolgeores.2008.05.010.
- 553 Takeuchi, S., Tomiya, A., Shinohara, H., 2009. Degassing conditions for permeable silicic
554 magmas: Implications from decompression experiments with constant rates. *Earth Planet.*
555 *Sci. Lett.* 283, 101–110. doi:10.1016/j.epsl.2009.04.001.
- 556 Toramaru, A., 2006. BND (bubble number density) decompression rate meter
557 for explosive volcanic eruptions. *J. Volcanol. Geotherm. Res.* 154, 303–316.
558 doi:10.1016/j.jvolgeores.2006.03.027.
- 559 Tuffen, H., Dingwell, D., Pinkerton, H., 2003. Repeated fracture and healing of silicic magma
560 generate flow banding and earthquakes? *Geology* 31, 1089–1092. doi:10.1130/G19777.1.
- 561 Webb, S.L., Dingwell, D.B., 1990. Non-Newtonian rheology of igneous melts at high stresses
562 and strain rates: Experimental results from rhyolite, andesite, basalt, and nephelinite. *J.*
563 *Geophys. Res.* 95, 15695–15701. doi:10.1029/JB095iB10p15695.
- 564 Woods, A.W., Koyaguchi, T., 1994. Transitions between explosive and effusive eruptions of
565 silicic magmas. *Nature* 370, 641–644. doi:10.1038/370641a0.
- 566 Wright, H.M.N., Cashman, K.V., Gottesfeld, E.H., Roberts, J.J., 2009. Pore structure of
567 volcanic clasts: Measurements of permeability and electrical conductivity. *Earth Planet.*
568 *Sci. Lett.* 280, 93–104. doi:10.1029/2006GL027224.
- 569 Wright, H.M.N., Roberts, J.J., Cashman, K.V., 2006. Permeability of anisotropic tube
570 pumice: Model calculations and measurements. *Geophys. Res. Lett.* 33, L17316.
571 doi:10.1016/j.epsl.2009.01.023.
- 572 Yokoyama, T., Takeuchi, S., 2009. Porosimetry of vesicular volcanic products by a water-
573 expulsion method and the relationship of pore characteristics to permeability. *J. Geophys.*
574 *Res.* 114, B02201. doi:10.1029/2008JB005758.

575 Yoshida, S., Koyaguchi, T., 1999. A new regime of volcanic eruption due to the relative mo-
576 tion between liquid and gas. *J. Volcanol. Geotherm. Res.* 89, 303–315. doi:10.1016/S0377-
577 0273(99)00005-0.

578 Zhang, Y., 1999. A criterion for the fragmentation of bubbly magma based on brittle failure
579 theory. *Nature* 402, 648–650. doi:10.1038/45210.

Table 1: Parameter space explored with the conduit model.

| parameter | symbol | value | unit |
|-----------------------------------|-------------|--------------------|----------------------------------|
| constants | | | |
| specific gas constant of water | R | 461.4 | $\text{J kg}^{-1} \text{K}^{-1}$ |
| Einstein constant | B | 2.5 | |
| constants equation (13) | c_1 | 0.9995 | |
| | c_2 | 0.4 | |
| | c_3 | 1 | |
| ash particle size | r_a | 1×10^{-3} | m |
| gas-wall drag coefficient | λ_w | 0.03 | |
| gas-ash particle drag coefficient | C_D | 0.8 | |
| textures | | | |
| bubble number density | N_d | 10^8 – 10^{16} | m^{-3} |
| tortuosity factor | m | 1–10 | |
| friction coefficient | f_0 | 10^{-4} – 10^2 | |
| throat-bubble ratio | f_{tb} | 0.05 – 0.5 | |
| conduit geometry | | MSH 1980 | SHV 1997 |
| length | L | 5291 | 5000 |
| radius | r_c | 30 | 22.5 |
| magma properties | | MSH 1980 | SHV 1997 |
| density | ρ_m | 2500 | 2450 |
| temperature | T | 1159 | 1123 |
| volatile content | c_0 | 4.6 | 4.6 |
| crystal content | χ_0 | 0.4 | 0.45 |
| pressure | P_0 | 140 | 120 |

Table 2: Values and range of dimensionless parameters.

| parameter | symbol | value | |
|-----------------------------------|----------|-----------------------|-----------------------|
| fixed parameters | | | |
| Reynolds number | Re | MSH 1980 6.69 | SHV 1997 0.27 |
| Froude number | Fr | 0.15 | 0.026 |
| Mach number | Ma | 0.0193 | 0.0033 |
| water content | c_0 | 0.046 | 0.046 |
| crystal content | χ_0 | 0.4 | 0.45 |
| fragmentation gas volume fraction | ϕ_f | 0.8 | 0.8 |
| density ratio | δ | 0.1 | 0.1 |
| saturation water content at P_0 | σ | 0.049 | 0.045 |
| ash/conduit size ratio | a_r | 3.33×10^{-5} | 4.44×10^{-5} |
| outgassing parameters | | | |
| Stokes number | St | $10^{-6} - 10^1$ | |
| Forchheimer number | Fo | $10^{-3} - 10^7$ | |

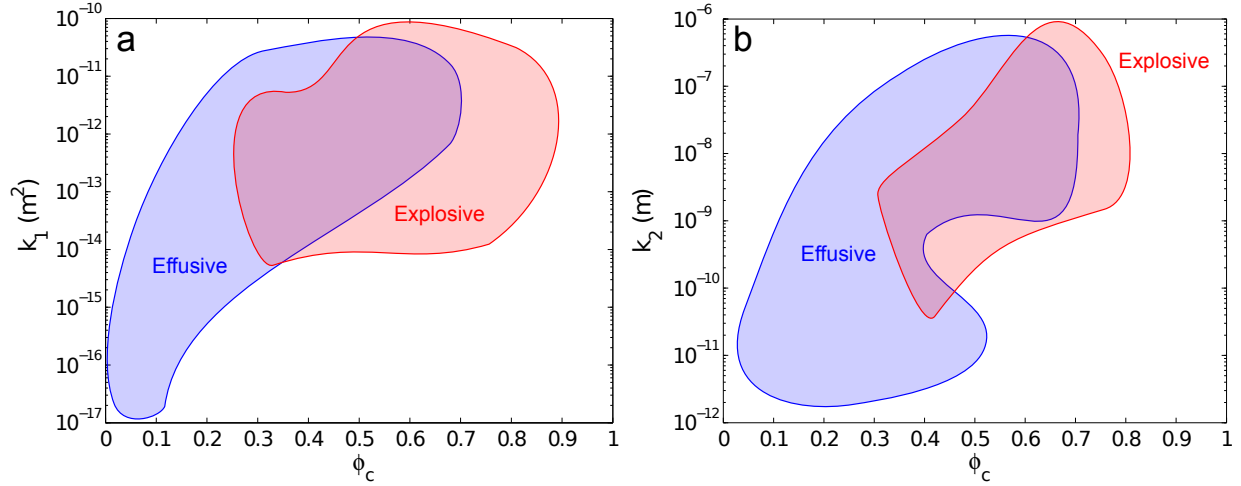


Figure 1: Summary of the relationship between of connected porosity ϕ_c and permeability. The blue area represents the spread in data collected on pyroclasts from effusive eruptions, the red area represents the data spread on pyroclasts from explosive eruptions for (a) Darcian permeability k_1 (Wright et al., 2009), and (b) inertial permeability k_2 (Rust and Cashman, 2004; Mueller et al., 2005; Takeuchi et al., 2008; Bouvet de Maisonneuve et al., 2009; Yokoyama and Takeuchi, 2009). Data from pyroclasts ejected by Vulcanian explosions are treated as effusive. Data are mostly from silica-rich pyroclasts, but also includes mafic products as porosity-permeability data does not appear to depend on composition.

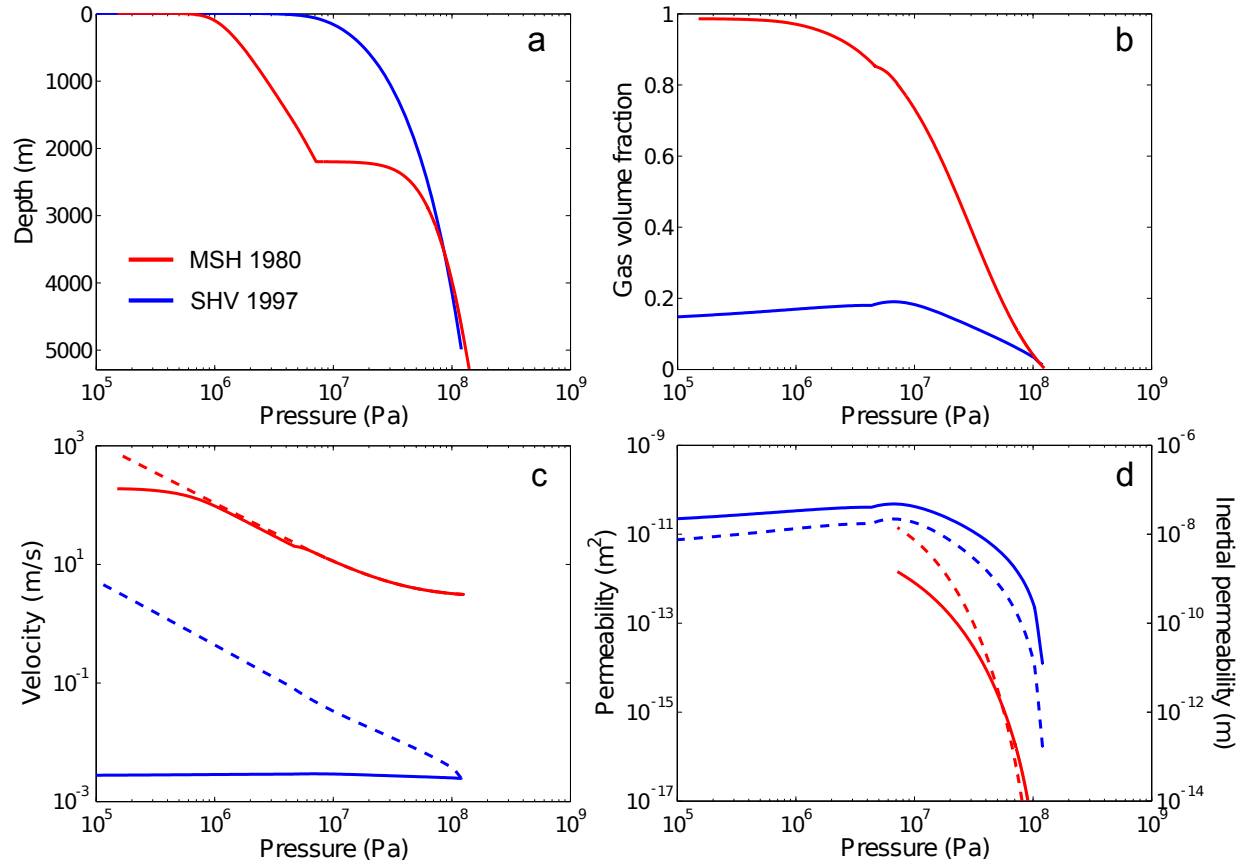


Figure 2: Illustrative solutions to the conduit model for MSH 1980 conditions with $N_d = 10^{15} \text{ m}^{-3}$, $m = 3.5$, $f_{tb} = 0.1$, $f_0 = 10$ (red) and SHV 1997 conditions with $N_d = 10^9 \text{ m}^{-3}$, $m = 2.2$, $f_{tb} = 0.3$, $f_0 = 10$ (blue) using a fragmentation criterion based on volume fraction. (a) depth versus pressure, (b) porosity versus pressure, (c) velocity versus pressure with the dashed curves indicating the gas velocity and the solid curves showing the magma velocity, and (d) the Darcian (solid curves) and the inertial permeability (dashed curves).

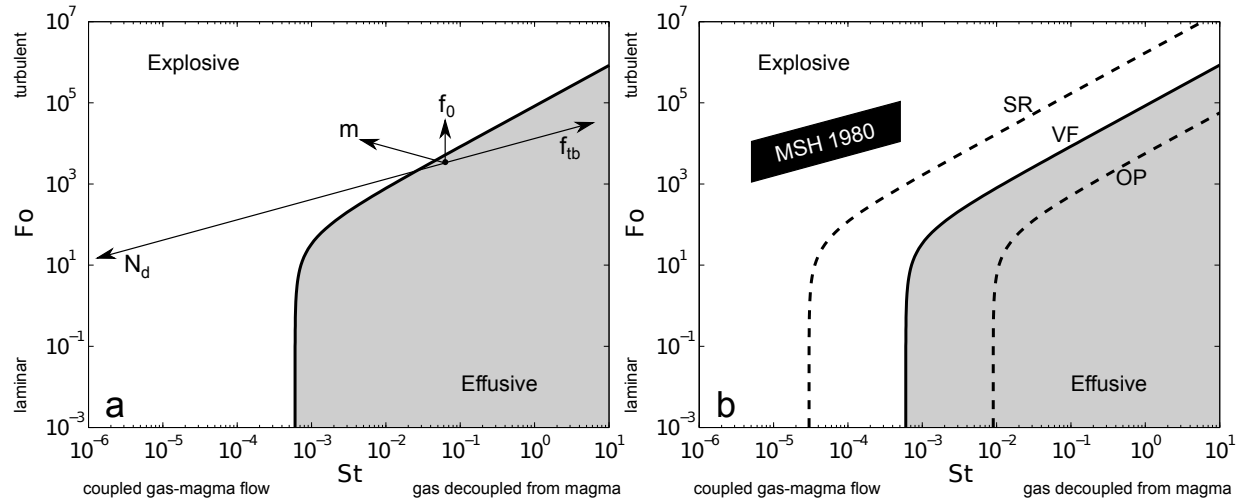


Figure 3: St-Fo map for the MSH 1980 magma properties and conduit geometry. The white area represents the explosive regime, and the grey area the effusive regime. (a) The arrows indicate how one travels on the map by increasing one of the textural properties starting from a randomly chosen point. The relative lengths of the arrows are determined by the range defined in Table 1. (b) The black area is defined by the textural properties found in the pyroclasts of the MSH 1980 eruption. It lies in the low St and high Fo region showing that the gas-magma flow was coupled and outgassing was turbulent. The dashed curves indicate the transition between effusive and explosive regimes for strain-rate fragmentation (SR) and overpressure fragmentation (OP), while the solid curve indicates fragmentation at a critical gas volume fraction (VF). See Appendix B for details on fragmentation criteria.

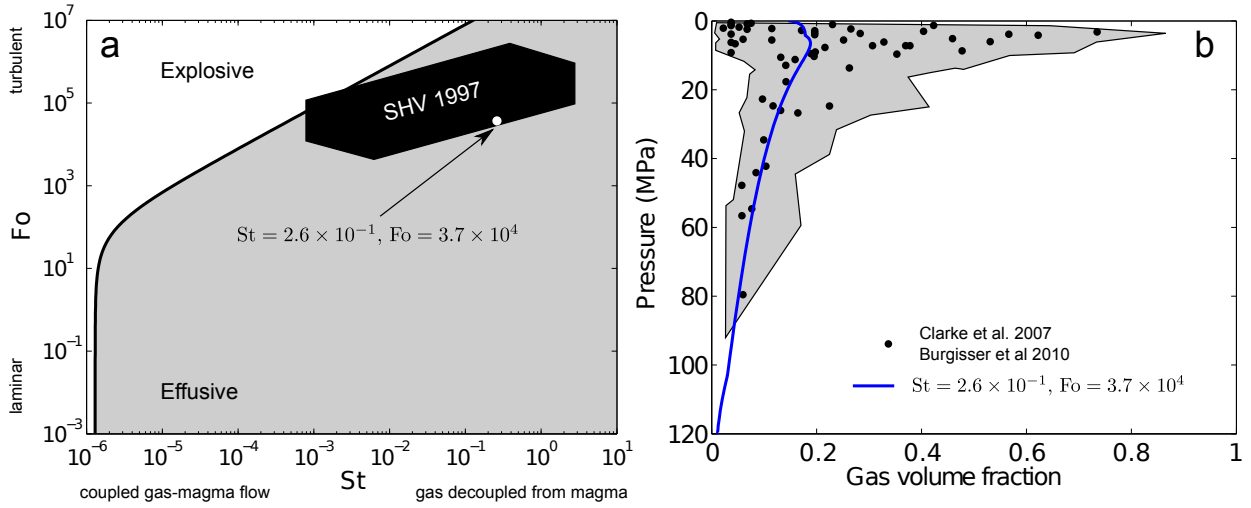


Figure 4: (a) St-Fo map for the SHV 1997 eruption conditions as determined from Monte Carlo simulations. The black area is defined by the textural properties found in the pyroclasts produced by the SHV 1997 eruptions. We can refine the black region to the white point by using the data points of pressure and gas volume fraction collected by Clarke et al. (2007) and Burgisser et al. (2010) in figure (b). The gray area in figure (b) represents the uncertainty in the model used by Burgisser et al. (2010) to obtain pre-explosive gas volume fraction. The blue line is the best fit of the model to this data for $P > 10$ MPa: $St = 2.6 \times 10^{-1}$, $Fo = 3.7 \times 10^4$, e.g. $N_d = 10^{9.5} \text{ m}^{-3}$, $f_{tb} = 10^{-0.5}$, $m = 2.1$, and $f_0 = 10$.

580 **Appendix A. Non-dimensionalization**

581 We scale the equations of the conduit model to permit better interpretation of the results.
 582 The model parameters can be divided into three main groups: (i) conduit geometry L, r_c ,
 583 (ii) magma properties $P_0, T, c_0, \phi_f, \rho_m, \chi_0$, and (iii) magma textures f_{tb}, f_0, N_d, m . From
 584 these parameters we define all other characteristic scales: a reference gas density

$$585 \quad \rho_{g0} = \frac{P_0}{RT}, \quad (\text{A.1})$$

586 a reference viscosity

$$587 \quad \log \mu_0 = -3.545 + 0.833 \ln 100c_0 + \frac{9601 - 2368 \ln 100c_0}{T - (195.7 + 32.25 \ln 100c_0)} \quad (\text{A.2})$$

$$588 \quad \theta_0 = \left\{ 1 - c_1 \operatorname{erf} \left(\frac{\sqrt{\pi}}{2} \chi_0 \left[1 + \frac{c_2}{(1 - \chi_0)^{c_3}} \right] \right) \right\}^{-B/c_1} \quad (\text{A.3})$$

$$589 \quad \mu_{l0} = \mu_0 \theta_0 \quad (\text{A.4})$$

591 a reference mass and volume flux

$$592 \quad q_0 = \frac{P_0 \rho_m r_c^2}{L 8 \mu_{l0}}, \quad U_0 = \frac{q_0}{\rho_m}, \quad (\text{A.5})$$

593 and the reference Darcian and inertial permeability

$$594 \quad k_{10} = \frac{\phi_f^m (f_{tb} r_{b0})^2}{8}, \quad (\text{A.6})$$

$$595 \quad k_{20} = \frac{(f_{tb} r_{b0}) \phi_f^{\frac{1+3m}{2}}}{f_0}, \quad (\text{A.7})$$

597 with

$$598 \quad r_{b0} = \left(\frac{\phi_f}{\frac{4\pi}{3} N_d (1 - \phi_f)} \right)^{1/3}. \quad (\text{A.8})$$

600 We then define the dimensionless quantities

$$601 \quad u'_m = \frac{u_m}{U_0}, \quad u'_g = \frac{u_g}{U_0}, \quad \rho'_g = \frac{\rho_g}{\rho_{g0}}, \quad \mu'_m = \frac{\mu_{l0}}{\mu_0}, \quad k'_1 = \frac{k_1}{k_{10}}, \quad k'_2 = \frac{k_2}{k_{20}}, \quad q' = \frac{q}{q_0} \quad (\text{A.9})$$

602 Substituting these in the conservation equations gives

$$603 \quad u'_m = \frac{1-n}{1-\phi} q' \quad (\text{A.10})$$

$$604 \quad \rho'_g u'_g = \frac{1-n}{\delta \phi} q' \quad (\text{A.11})$$

$$605 \quad u'_m \frac{du'_m}{dz'} = -\frac{3}{4} \delta \frac{1}{\text{Ma}^2} \frac{dP'}{dz'} - \frac{1}{\text{Fr}^2} + \frac{F'_{mg}}{1-\phi} - \frac{F'_{mw}}{1-\phi} \quad (\text{A.12})$$

$$606 \quad \rho'_g u'_g \frac{du'_g}{dz'} = -\frac{3}{4} \frac{1}{\text{Ma}^2} \frac{dP'}{dz'} - \frac{1}{\text{Fr}^2} \rho'_g - \frac{1}{\delta} \frac{F'_{mg}}{\phi} - \frac{F'_{gw}}{\phi} \quad (\text{A.13})$$

$$607 \quad F'_{mg} = \begin{cases} \frac{1}{\text{St}} \left(1 + \text{Fo} \frac{k'_1}{k'_2} \rho'_g |u'_g - u'_m| \right) \frac{\phi(1-\phi)}{k'_1} (u'_g - u'_m) & \phi \leq \phi_t \\ \left(\frac{1}{k'_1 \text{St}} \left(1 + \text{Fo} \frac{k'_1}{k'_2} \rho'_g |u'_g - u'_m| \right) \right)^{1-t} \left(\frac{3}{8} \frac{1}{a_r} C_D \rho'_g |u'_g - u'_m| \right)^t \phi(1-\phi)(u'_g - u'_m) & \phi_t < \phi \leq \phi_f \\ \frac{3}{8} \frac{1}{a_r} C_D \rho'_g \phi(1-\phi) |u'_g - u'_m| (u'_g - u'_m) & \phi > \phi_f \end{cases} \quad (\text{A.14})$$

$$608 \quad F'_{mw} = \begin{cases} \frac{8\mu'_m u'_m}{\text{Re}} & \phi \leq \phi_f \\ 0 & \phi > \phi_f \end{cases} \quad (\text{A.15})$$

$$609 \quad F'_{gw} = \begin{cases} 0 & \phi \leq \phi_f \\ \frac{\lambda_w}{4} \rho'_g u'^2_g & \phi > \phi_f \end{cases} \quad (\text{A.16})$$

$$610 \quad n = \frac{c_0 - \sigma P^{1/2}}{1 - \sigma P^{1/2}} \quad (n \geq 0), \quad (\text{A.17})$$

612 with Re the Reynolds number of the magma phase,

$$613 \quad \text{Re} = \frac{\rho_m r_c U_0}{\mu_{l0}}, \quad (\text{A.18})$$

614 Ma the Mach number of the gas phase (water),

$$615 \quad \text{Ma} = \frac{U_0}{\sqrt{\frac{4}{3} RT}}, \quad (\text{A.19})$$

616 Fr the Froude number,

$$617 \quad \text{Fr} = \frac{U_0}{\sqrt{g r_c}}, \quad (\text{A.20})$$

618 δ the density ratio between the gas and the magma phase,

$$619 \quad \delta = \frac{\rho_{g0}}{\rho_m}, \quad (\text{A.21})$$

620 σ the saturation water content at initial pressure P_0 ,

$$621 \quad \sigma = sP_0^{1/2}, \quad (\text{A.22})$$

622 and a_r the ratio between the ash size and the conduit radius,

$$623 \quad a_r = \frac{r_a}{r_c}. \quad (\text{A.23})$$

624 St is the Stokes number, the ratio of the response time scale of the magma and the charac-
625 teristic flow time of the gas

$$626 \quad \text{St} = \frac{\tau_V}{\tau_F} = \frac{\frac{\rho_m k_{10}}{\mu_g}}{\frac{r_c}{U_0}} \quad (\text{A.24})$$

627 and Fo is the Forchheimer number the ratio of the inertial term and the viscous term in
628 Forchheimer's equation

$$629 \quad \text{Fo} = \frac{\rho_{g0} k_{10} U_0}{k_{20} \mu_g}. \quad (\text{A.25})$$

630 From this scaling analysis we find two parameters that are influenced by textures, St and
631 Fo. When keeping the conduit geometry and magma properties constant only St and Fo will
632 vary, while others remain constant (Table 2). Therefore, the textural control on the effusive-
633 explosive transition can be projected onto a St-Fo plane. We create such a St-Fo map for two
634 case studies by doing Monte Carlo simulations within the defined texture parameter space
635 (Table 1).

636 **Appendix B. Fragmentation mechanisms**

637 We investigate the effect of different fragmentation mechanisms on the results, using
638 either a criterion based on (i) critical strain-rate, (ii) overpressure or (iii) volume fraction.
639 The strain-rate criterion was defined by Dingwell (1996) and Papale (1999) as

$$640 \quad \frac{du_m}{dz} > 0.01 \frac{G}{\mu_m}, \quad (\text{B.1})$$

641 with $G = 10$ GPa. Note that we use the elongational strain-rate and not the shear-strain
642 rate, which cannot be assessed by a one-dimensional model (Gonnermann and Manga, 2003).
643 Overpressure cannot be directly calculated in our model as the pressure between both phases

644 is at equilibrium. However, we assume the overpressure can be quantified by the dynamic
645 pressure induced by the interphase drag between the two phases

$$646 \quad \frac{dP_{\Delta}}{dz} = F_{mg} \quad (\text{B.2})$$

647 Integrating this equation along with the governing conservation equations gives us an esti-
648 mate of the overpressure P_{Δ} in the bubble network. Following Zhang (1999), fragmentation
649 occurs when

$$650 \quad P_{\Delta} > \frac{2(1 - \phi)}{(1 + 2\phi)} P_c \quad (\text{B.3})$$

651 where we used $P_c = 100$ MPa (Webb and Dingwell, 1990). Our results show a shift in
652 the transition curve (Figure 3b), but do not produce any qualitative difference in the re-
653 sults. These findings are in agreement with other studies comparing different fragmentation
654 mechanisms (Melnik and Sparks, 2002b; Massol and Koyaguchi, 2005).